Computer Networks 103 (2016) 196–206

Contents lists available at ScienceDirect

Computer Networks

journal homepage: www.elsevier.com/locate/comnet

Assessing network robustness under SIS epidemics: The relationship between epidemic threshold and viral conductance

A. Socievole[a,*], F. De Rango[a], C. Scoglio[b], P. Van Mieghem[c]

[a] Department of Informatics, Modeling, Electronics and Systems Engineering, University of Calabria, Cubo 41 C, Ponte P. Bucci, 87036, Arcavacata di Rende (CS), Italy
[b] Department of Electrical and Computer Engineering, Kansas State University, KS 66506, Manhattan, USA
[c] Faculty of Electrical Engineering, Mathematics and Computer Science, Delft University of Technology, 2600 GA, Delft, The Netherlands

ARTICLE INFO

Article history:
Received 11 September 2015
Revised 14 March 2016
Accepted 20 April 2016
Available online 26 April 2016

Keywords:
Network robustness
Viral conductance
Epidemic threshold
SIS epidemics
NIMFA model

ABSTRACT

Telecommunication networks, as well as other network types, are critical infrastructures where any service disruption has a notable impact on individuals. Hence, studying network dynamics under failures or attacks is of paramount importance. In this paper, we assess the robustness of networks with respect to the spread of Susceptible-Infected-Susceptible (SIS) epidemics, using the N-Intertwined Mean-Field Approximation (NIMFA). A classical robustness metric is the NIMFA epidemic threshold, which is inversely proportional to the largest eigenvalue of the adjacency matrix, also called the spectral radius. Besides the NIMFA epidemic threshold, the viral conductance has been proposed as a measure incorporating the average fraction of infected nodes in the steady state for all possible effective infection rates. In general, the viral conductance provides more information about the network's behavior with respect to virus spreading, however, the full picture is not always necessary. The aim of this paper is to understand when the spectral radius is adequate for reflecting robustness. By analyzing the relationship between spectral radius and viral conductance in several graph classes, we show that the two metrics are highly correlated. We thus conclude that the spectral radius is sufficient to compare the robustness of networks belonging to the same class.

1. Introduction

Much effort has been devoted in the analysis of the spread of epidemics, mainly due to the expected outbreak of new lethal biological viruses affecting individuals and the increasing threats from cybercrime. In November 2014, for example, the Ebola epidemic caused 9596 laboratory-confirmed cases of individuals infected by the virus with 5459 total deaths, becoming the largest epidemic in history affecting multiple countries in West Africa. In addition to epidemic spread among individuals, there are other important scenarios like telecommunication systems, power grids and transportation networks, where the theory of the spread of epidemics can be applied to characterize their vulnerability. E-mail worms, computer viruses, the propagation of failures in power grids, and, more generally, the spread of information and epidemic dissemination/routing in ah-hoc and peer-to-peer networks are just some examples of scenarios, where studying the spread of epidemics is crucial for maintaining high levels of robustness. Assessing network robustness not only allows us to compare the robustness among different network topologies, but also gives insights in the design of future networks to mitigate the spreading of a virus or cascading failures, or maximize information diffusion (e.g. news, rumors, brand awareness, marketing of new products, etc.).

In this paper, we focus on the spread of epidemics on telecommunication networks. Network operators are mainly interested in understanding (a) how much robust their network is compared to other networks and (b) how to protect or modify their infrastructure for improving its robustness minimizing costs. The aim of this paper is to answer the first question focusing on the spread of epidemics described through a Susceptible-Infected-Susceptible (SIS) model [1]. This model, which arose in mathematical biology, and its variants, are often used for the spread of viruses and malwares in computer networks [2–4], and mobile social opportunistic networks [5], epidemic information dissemination in unreliable distributed systems like P2P and ad-hoc networks [6], cascading failures on BGP networks [7] and power grids [8], smartphone malware propagation [9], and epidemic spreading in

* Corresponding author.
E-mail addresses: socievolea@dimes.unical.it (A. Socievole), derango@dimes.unical.it (F. De Rango), caterina@ksu.edu (C. Scoglio), P.F.A.VanMieghem@tudelft.com (P. Van Mieghem).

http://dx.doi.org/10.1016/j.comnet.2016.04.016
1389-1286/

wireless sensor networks [10]. A network is represented by an undirected graph $G(N, L)$, characterized by a symmetric adjacency matrix A in which the element $a_{ij} = a_{ji} = 1$ if there is a link between nodes i and j, otherwise $a_{ij} = 0$. The infectious state of a node i in G is specified by a Bernoulli random variable $X_i \in \{0, 1\} : X_i = 0$ for a *healthy* node and $X_i = 1$ for an *infected* node. A node i at time t can be in the infected state, with probability $v_i(t) = \Pr[X_i(t) = 1]$, or in the healthy state, with probability $1 - v_i(t)$. Both the arrival of an infection over a link and the curing of an infected node i are assumed to be independent Poisson processes with rates β and δ, respectively, and the effective spreading rate is defined as $\tau = \frac{\beta}{\delta}$. This SIS model can be expressed exactly in terms of a continuous-time Markov chain with 2^N states as shown in [11]. Since the exact solution $v_i(t)_{1 \le i \le N}$ for any network is intractable, several approximations of the SIS model have been proposed. In this paper, we focus on the N-Intertwined Mean-Field Approximation (NIMFA) [11] that was earlier considered in discrete time in [12] and in [13], whose paper was later improved in [14]. NIMFA has been shown in [15] to be better than the widely used heterogeneous mean-field model of Pastor-Satorras and Vespignani [16].

A remarkable property of the SIS model is the existence of a phase transition [16] when the effective spreading rate approaches an epidemic threshold τ_c: if $\tau > \tau_c$, the infection becomes persistent, while if $\tau < \tau_c$, the virus dies out and the network is virus-free. Many authors (see, e.g., [2,17–19]) mentioned the existence of an *epidemic threshold*, however, the determination of this epidemic threshold is a long-standing open problem and a major contribution of NIMFA is the lower bound $\tau_c^{(1)} = \frac{1}{\lambda_1} \le \tau_c$, where $\tau_c^{(1)}$ is the NIMFA epidemic threshold and λ_1 is the largest eigenvalue of the network adjacency matrix A, also called the spectral radius. The NIMFA epidemic threshold has been used as a measure for network robustness [20]. Recently, the *viral conductance*, introduced in [21,22] and analyzed in depth in [23], was proposed as a robustness measure considering both the value of the epidemic threshold and the number of infected nodes at the steady state above the threshold. The viral conductance measures the integrated effect over all possible viral infection strengths on the network's infectious vulnerability and is shown to be a better robustness measure than the epidemic threshold, considering that viral conductance provides more information about the system's behavior [22].

In this paper, we present an extensive analysis on the relationship between the viral conductance and the spectral radius[1] in telecommunication networks. We chose to model the relationship between epidemic threshold and viral conductance for the SIS model since these two robustness metrics have been defined for this epidemic model. For the SIR model, for example, which is variant of the SIS model having a third state where a node can be recovered (R), there exist similar bounds for the epidemic threshold [24] but there is not yet an expression for the viral conductance. This is the reason why we start analyzing the SIS model and leave the study of the relationship between the two robustness metrics in other epidemic models to future investigations. The aim of this analysis is to understand if both the two metrics are necessary for characterizing the robustness of a network with respect to the spreading of a virus. In particular, we have chosen to test a set of topologies to model the most widely diffused telecommunication networks (e.g. complete bipartite graphs for core telecommunication networks, Erdős–Rényi random graphs [25] for peer-to-peer and ad hoc networks, Watts–Strogatz small-world graphs [26] for mobile contact networks, Bárabasi–Albert [27] scale-free graphs for social networks, etc.) and a set of real-world Internet backbones. The contributions of this paper can be summarized as follows:

- we derive easy to use upper and lower bounds for the viral conductance as a function of the spectral radius;
- via examples, we show cases where both the viral conductance and the spectral radius correctly compare the robustness between two networks, and cases where the spectral radius fails to assess robustness;
- we consider several graph classes representative of different types of networks and derive the relationship between the viral conductance and the spectral radius analytically, where possible, or through a correlation analysis;
- we show that the two metrics are highly correlated and hence, the information provided by the spectral radius is adequate for comparing the robustness of networks belonging to the same graph class.

The rest of this paper is organized as follows. Section 2 reviews the literature and related works. Section 3 reviews NIMFA. The viral conductance measure is described in Section 4. Section 5 compares the viral conductance and the epidemic threshold through case studies. Section 6 and 7 analyze the relationship between the viral conductance and the spectral radius in various graph classes. Conclusions are summarized in Section 8.

2. Related works

The spread of information or viruses, or the propagation of failures in communication networks are similarly described as the virus spread in a biological population [28]. Biological epidemic models were initiated by Kephart and White [2], for example, to describe the spread of viruses in computer networks. In classical epidemiology, epidemic models such as [1,29] introduced the basic reproductive number R_0 representing the average number of infections due to a single infected case in the population. For $R_0 < 1$, the epidemic dies out without causing an outbreak while for $R_0 > 1$, the epidemic spreads in the population. The basic reproductive number R_0 bears some resemblance with the epidemic threshold [16] defined in complex network theory for SIS epidemic models using the heterogeneous mean-field approach. However, the basic reproductive number R_0 does not contain any information about the underlying contact network. Since the structure of networks is rich and complex, R_0 is inadequate for assessing the threshold behavior of an outbreak in most networks.

In the literature dealing with the epidemic threshold in networks, Wang et al. [13] proposed a discrete-time epidemic model to predict the infection size within a population suggesting that the epidemic threshold equals the reciprocal of the spectral radius of the adjacency matrix A. In another work, Van Mieghem et al. [11] studied SIS epidemics as a continuous-time Markov chain and introduced NIMFA, whose epidemic threshold was proved to be equal to the inverse of the spectral radius of A. In [30], an heterogeneous version of NIMFA was used to design a strategy for controlling an epidemic outbreak in an arbitrary contact network by distributing vaccination resources throughout the network. More recently, NIMFA has been extended to model the SIS epidemic spread in networks of individuals partitioned into communities [31,32], where the infection rate by which an individual infects individuals in its own community is different from the inter-community infection rate. In another recent work [33] , NIMFA has been used to design resilient and secure networks for cyber attack-induced cascading link failures in critical infrastructures.

The epidemic threshold was initially used to assess network robustness with respect to the spread of epidemics [20]: the larger

[1] For the easier readability of the results obtained in this work, we consider the reciprocal of the NIMFA epidemic threshold (i.e. the spectral radius) when analyzing in deep the relationship between the two robustness metrics.

the epidemic threshold, the more robust a network is against the spread of an epidemic. Later, the viral conductance [21–23] was proposed as a robustness measure integrating the fraction of the infected nodes at the steady state for all possible infective infection strengths that an epidemic may possess. In this work, the authors also introduced a computational heuristic for the viral conductance, which is a function of the infected population and the network characteristics. Complementarily to viral conductance, *epidemic criticality* (EC) [34] was recently proposed as robustness metrics for epidemic-like failure scenarios. While viral conductance takes into account the fraction of infected nodes in the steady state and considers several epidemic intensities, EC focuses on the individual probability to be infected of each node and takes into account only one epidemic intensity. In the case where two topologies have the same viral conductances, EC would be able to detect which of the two topologies would have a higher percentage of critical nodes. Another network robustness metric was proposed by Trajanovski et al. [35] in a work defining a temporal robustness metric on time-varying networks. Results on real-world networks show that temporal connectivity is significantly more affected by intelligent attacks than random failures. On the contrary, random errors and intelligent attacks exhibit a similar behavior on randomly generated networks. In another work, Trajanovski et al. [36] considered the problem of improving network robustness in relation to the geographical embedding of a network. First, they focused on finding a circular region with radius r that would cause the biggest network degradation when removing all the covered nodes. Then, they also proposed a region-aware network augmentation strategy proving on a set of real-world backbones that adding few links may already induce significant robustness gains. In addition, they proposed an algorithm for finding two paths with minimum total weight between the source and the destination node that can not be cut by a singular circular region failure of radius r and to be used to reroute traffic after a regional failure.

In addition to the aforementioned works proposing single robustness metrics, some works like [37–39] proposed the aggregation of more robustness metrics into a single robustness value identifying a network. In [37], for example, a framework for computing network robustness was proposed in order to compare different networks against various topological perturbations by using the R value characterizing each network. Here, the R value ranges between [0, 1] and is computed through a weighted linear model taking into account several metrics that characterize the graph representing the network (e.g. average hop count, minimum degree, maximum degree, and so on). The higher the R value, the larger the robustness. The same R value has been used in [39] to study network robustness in real and random networks through an envelope approach. Under node removal, considering both random node failure and targeted node attacks based on network centrality metrics, this approach shows that although networks may have similar average-case performance under attack, they may differ significantly in their sensitivities to certain attack sequences. Similarly in [38], the concept of robustness surface embracing more robustness metrics was introduced in order to visually assess the network robustness variability.

In summary, there exist different ways to measure network robustness. Specifically, when dealing with epidemic spreads that are the focus of this paper, epidemic threshold and viral conductance are commonly used. Moreover, some works in the literature combine more robustness metrics to define a unique robustness value representing a network. However, since most of the robustness metrics are computed from the adjacency matrix of the graph representing the network, we may expect that most metrics are dependent thus being redundant. As such, we study the relationship between epidemic threshold and viral conductance showing that the two metrics are highly correlated in several graph classes. We finally conclude that the more complete information provided by the viral conductance is not always necessary.

3. The SIS N-Intertwined Mean-Field Approximation (NIMFA)

Although a SIS epidemic process is an abstraction of how a real virus spreads on a contact network, the SIS model is still too complex for a general analytic treatment as shown in [11]. As such, the behavior of SIS epidemics on networks is often analyzed approximately, using a variant of a mean-field approach such as the N-intertwined mean-field approximation (NIMFA). In NIMFA, the probability for node i of being infected $v_i(t)$ is described by

$$\frac{dv_i(t)}{dt} = \beta(1 - v_i(t)) \sum_{j=1}^{N} a_{ij} v_j(t) - \delta v_i(t) \tag{1}$$

The time-derivative in Eq. (1) of the probability $v_i(t)$ depends on two competing processes: (a) while healthy with probability $(1 - v_i(t))$, the infected neighbors of node i, whose average number is $\sum_{j=1}^{N} a_{ij} v_j(t)$, try to infect i with rate β and (b) while infected with probability $v_i(t)$, node i is cured with rate δ. By introducing the vector $V(t) = \begin{bmatrix} v_1(t) & v_2(t) & \dots & v_N(t) \end{bmatrix}^T$, the differential Eq. (1) can be written in matrix form as

$$\frac{dV(t)}{dt} = (\beta A - \delta I)V(t) - \beta \mathrm{diag}(v_i(t))AV(t) \tag{2}$$

where I is the identity matrix, $\mathrm{diag}(v_i(t))$ is the diagonal matrix whose diagonal elements are $v_1(t)$, $v_2(t)$, ...,$v_N(t)$ and A is the adjacency matrix of the network. Focusing on the NIMFA steady state (supposing a steady state depending on the initial values of $V(t)$ exists), which is defined by $v_{i\infty} = \lim_{t\to\infty} v_i(t)$ or $\lim_{t\to\infty} \frac{dv_i(t)}{dt} = 0$ and which corresponds to the metastable state in the exact Markovian SIS model, by passing to the limit in Eq. (1), we obtain for each node i

$$\beta \sum_{j=1}^{N} a_{ij} v_{j\infty} - v_{i\infty} \left(\beta \sum_{j=1}^{N} a_{ij} v_{j\infty} + \delta \right) = 0 \tag{3}$$

Since the matrix A has all the diagonal elements equals to 0, $a_{jj} = 0$, the steady-state probability $v_{i\infty}$ can be written as

$$v_{i\infty} = \frac{\beta \sum_{j=1}^{N} a_{ij} v_{j\infty}}{\beta \sum_{j=1}^{N} a_{ij} v_{j\infty} + \delta} = 1 - \frac{1}{1 + \tau \sum_{j=1}^{N} a_{ij} v_{j\infty}} \tag{4}$$

which is the ratio between the mean infection rate caused by the node's infected neighbors and the total mean rate of both the competing infection and curing process. The trivial solution of Eq. (4) is $v_{i\infty} = 0$ for all i (i.e., the overall-healthy state), which corresponds to the absorbing state of the SIS Markov chain and reflects the steady state of the exact SIS model.

In NIMFA, the largest eigenvalue λ_1 of the graph's adjacency matrix A rigorously defines the first order epidemic threshold $\tau_c^{(1)} = \frac{1}{\lambda_1}$. A second-order epidemic threshold $\tau_c^{(2)} \leq \tau_c^{(1)}$ has been studied in [40] which also presents a different derivation of the N-intertwined equations. In [11] and [40], it is proven that a major property of the N-intertwined approximation is that $V_i(t) \geq V_i(t)|_{exact}$. Hence, NIMFA upper-bounds the SIS epidemics and, consequently, $\tau_c^{(1)} \leq \tau_c$. Further details on the properties of NIMFA approximation and its relationship with the characteristics of the SIS model can be found in [41].

4. The viral conductance

The viral conductance, proposed in [21] as a robustness graph measure, is defined as

$$\psi = \int_0^{\lambda_1} y_\infty(s) ds \tag{5}$$

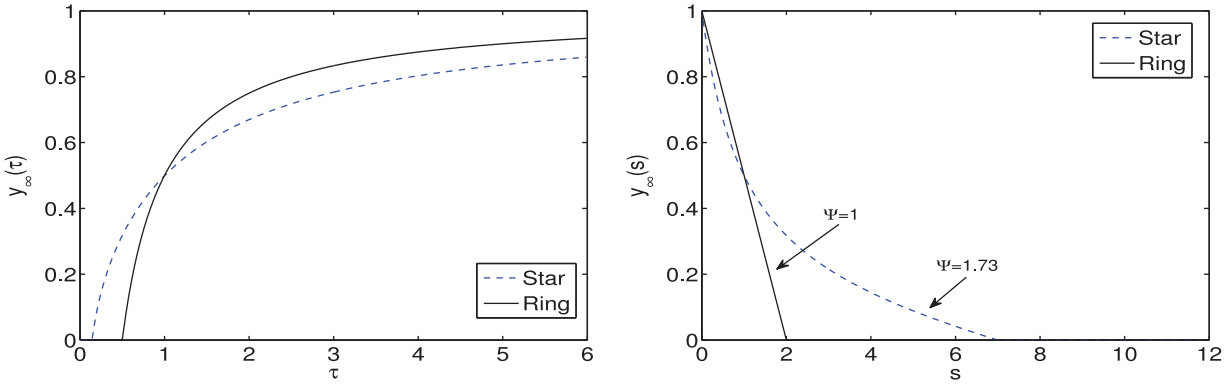

(a) (b)

Fig. 1. The NIMFA average steady-state fraction of infected nodes in a star and a ring graph with $N = 50$ nodes versus (a) τ and (b) $s = 1/\tau$. The two graphs have similar average degree.

where $y_\infty = \frac{1}{N}\sum_{i=1}^{N} \nu_{i\infty}$ is the average fraction of infected nodes in the steady state and $s = \frac{1}{\tau}$. For $\tau < \tau_c$ and equivalently, for $s > \frac{1}{\tau_c} = \lambda_1$, the network is virus-free in the steady state. Since $y_\infty(\tau)$ is not integrable over all τ, the viral conductance was defined in terms of $y_\infty(\frac{1}{\tau})$. Fig. 1(a) and Fig. 1(b) show the NIMFA average steady-state fraction of infected nodes as a function of τ and $s = \frac{1}{\tau}$ respectively, for a star and a ring graph with $N = 50$ nodes.

In most papers on virus spread, the robustness of a network against virus spread is measured by the epidemic threshold. Given two networks, the network with the highest epidemic threshold is considered more robust and, hence, more resistant to the virus. According to this criterion, the ring graph in Fig. 1(a) is more robust against virus propagation than the star, because the ring graph has a higher epidemic threshold. However, Fig. 1(a) illustrates that for $\tau > 1$, the ring graph has a larger average fraction of infected nodes and hence, it is more vulnerable than the star graph. Once the epidemic threshold is crossed, the virus behaves differently in networks with low and high epidemic thresholds. Motivated by this consideration, Kooij et al. [21] proposed the viral conductance as an additional robustness measure accounting for the conductance of the virus for all possible infection rates: given two graphs G_1 and G_2, the graph G_1 is considered more robust than the graph G_2 if $\psi_{G_1} < \psi_{G_2}$. Hence, considering Fig. 1(b), the ring graph is more robust against virus propagation than the star, since it has a lower viral conductance.

In [23], exact expressions for the viral conductance were derived. For regular graphs with degree d and L links, the viral conductance equals

$$\psi_{regular} = \int_0^d \left(1 - \frac{s}{d}\right) ds = \frac{d}{2} = \frac{L}{N} \tag{6}$$

which is independent of the number of nodes N. The ring, which is an example of a regular graph with $d = 2$, has $\psi_{ring} = 1$, irrespective of the number of nodes N. For complete bipartite graphs $K_{m,n}$, the exact expression of the viral conductance is

$$\psi_{K_{m,n}} = \sqrt{mn} - \frac{mn}{N} + \frac{n-m}{N} \ln \frac{(1+\sqrt{n/m})^m}{(1+\sqrt{m/n})^n} \tag{7}$$

which is symmetric, so that $\psi_{K_{m,n}} = \psi_{K_{n,m}}$.

Sharp bounds for the lower and upper bound of the viral conductance ψ exist,

$$Z + \zeta(1-Z) + K_{min} \le \frac{\psi}{\frac{\lambda_1}{2}} \le Z + \zeta(1-Z) + K_{max} \le 1$$

where $Z = \frac{1}{N}\frac{\sum_{j=1}^{N}(x_1)_j}{\sum_{j=1}^{N}(x_1)_j^3} \le 1$ with $(x_1)_j$ the j-th vector component of the principal eigenvector x_1 of A belonging to the eigenvalue λ_1 (also known as eigenvector centrality [42] of j-th node) and $\sum_{j=1}^{N}(x_1)_j = w_1$ the fundamental weight [43], and where $\zeta = \frac{1-Z}{|\lambda_1 E[\frac{1}{D}] - Z|} \le 1$, but $K_{min} \ge 0$ and $K_{max} \ge 0$ are more complicated to evaluate (see [23, Eq. (39) and (40)]). Therefore, we limit ourselves to the slightly worse lower bound in which we consider the lowest possible value for K_{min} obtaining

$$\psi_{LB} = \frac{\lambda_1}{2}(Z + \zeta(1-Z)) \tag{8}$$

and the upper bound (proved in [23])

$$\psi_{UB} = \frac{\lambda_1}{2} \tag{9}$$

Combining Eqs. (8) and (9) leads to

$$Z + \zeta(1-Z) \le \frac{\psi}{\frac{\lambda_1}{2}} \le 1 \tag{10}$$

which shows that, the closer $Z + \zeta(1-Z)$ is to 1, the closer the viral conductance is to Eq. (9).

5. Viral conductance versus epidemic threshold

In the example shown in Fig. 1, the two robustness metrics lead to the same conclusion: both $\tau_c^{(1)} = \frac{1}{\lambda_1}$ and ψ consider the ring graph more robust than the star graph. However, there are cases in which the epidemic threshold fails to assess the robustness of networks. Fig. 2 shows an example of two networks, a star graph G_1 with $N_1 = 62$ nodes and an Erdős–Rényi random graph [25] G_2 with $N_2 = 50$ nodes and edge probability $p = 0.15$, having $L_1 > L_2$ and almost the same NIMFA epidemic threshold. According to the robustness criterion based on the epidemic threshold, the two networks have almost the same robustness. However, for $\tau > \tau_c^{(1)}$, the star graph has an average fraction of infected nodes lower than the Erdős–Rényi random graph. This behavior is well reflected by the viral conductance which is higher for the Erdős–Rényi random graph (Fig. 2(b)) and properly assesses that the star graph is more robust than the Erdős–Rényi random graph. Similar examples showing networks with the same epidemic threshold and different viral conductance can be found in [22] and in [21].

There are other cases in which the two metrics answer differently to the question "Which network is the most robust?". In [21], the viral conductance of some real-life networks and synthetic networks with approximately 1000 nodes is computed. For example, the Abilene backbone network [21] has $\tau_c = 0.11$ and $\psi = 1.43$, while the Stanley Ring network has $\tau_c = 0.14$ and $\psi = 1.79$. If we compare the two networks with respect to the epidemic threshold,

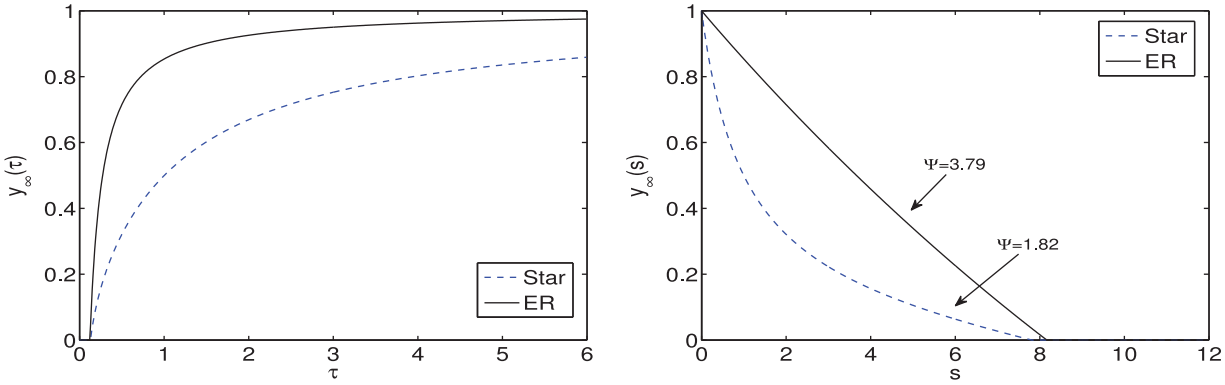

(a) (b)

Fig. 2. The NIMFA average steady-state fraction of infected nodes in a star with $N = 62$ nodes and an Erdős–Rényi random graph with $N = 50$ nodes and edge probability $p = 0.15$ versus (a) τ and (b) $s = 1/\tau$. The two graphs have almost the same epidemic threshold but different viral conductance.

we conclude that the Stanley Ring network is the most robust. On the contrary, if we compare them with respect to the viral conductance, we conclude that the Abilene network is the most robust. In general, we consider the viral conductance as the most reliable, viral robustness measure since it incorporates the fraction of infected nodes at the steady state for all effective infection strengths.

The previous examples illustrated cases in which both the epidemic threshold and the viral conductance similarly assess the robustness of networks and cases in which the epidemic threshold is not an adequate measure of network robustness. However, for most networks, we cannot analytically compute the fraction of infected nodes $y_\infty(s)$ nor the viral conductance explicitly. Therefore, we use numerical analysis to determine the steady-state values for the fraction of infected nodes, for a given value of s. The average fraction $y_\infty(s)$ of infected nodes is evaluated for 100 equidistant values of s, between 0 and λ_1. Finally, the viral conductance ψ is determined approximating the integral of $y_\infty(s)$ via the trapezoidal method. Here, we are interested in finding particular cases where the more complete information about network's behavior given by the viral conductance is not necessary and the robustness of two different graphs can be assessed by the spectral radius. Thus, we state:

Intra-class Network Robustness Hypothesis: the robustness of networks belonging to the same class can be assessed by the spectral radius.

This hypothesis is verified in the following section for different network classes.

6. Relationship between robustness metrics in graphs with exact expressions for ψ

In this section, we start analyzing the relationship between the viral conductance and the spectral radius for the regular graph and the complete bipartite graph. Specifically, we show the relationship between ψ and λ_1 by reporting the expression of ψ as a function of λ_1.

6.1. Regular graphs

In a regular graph, every node has the same degree d. Since the spectral radius for a regular graph is $\lambda_1 = d$ (see [42]), the viral conductance Eq. (6) can be written as

$$\psi_{regular} = \frac{d}{2} = \frac{\lambda_1}{2} \tag{11}$$

so that the viral conductance for the regular graph is half of the spectral radius, and equivalently, half of the inverse of the epidemic threshold.

6.2. Complete bipartite graphs

The complete bipartite graph $K_{m,n}$ is characterized by two partitions P_m and P_n containing respectively m and n nodes, forming a graph with $N = m + n$ nodes. All nodes of the partition P_m are connected to all the nodes of P_n, while nodes belonging to the same partition do not connect. Core telecommunication networks are often modeled as complete bipartite graphs for their robustness against link failures. For example, the Amsterdam Internet Exchange[2], one of the largest Internet exchange points in the world, uses this topology. Also sensor networks are often modeled by $K_{m,n}$.

Since the spectral radius for the $K_{m,n}$ graph [42] is $\lambda_1 = \sqrt{mn}$, the exact expression of the viral conductance can be written as

$$\psi_{K_{m,n}} = \lambda_1 \left(1 - \frac{\lambda_1}{N}\right) + c_{m,n} \tag{12}$$

where

$$c_{m,n} = \frac{n-m}{N} \ln \frac{(1+\sqrt{n/m})^m}{(1+\sqrt{m/n})^n} \tag{13}$$

is an asymmetry correction. For $m = n$, we obtain a regular graph Eq. (6).

A particular complete bipartite graph is the star graph where $m = 1$ and $n = N - 1$. For any connected graph, an upper bound for the spectral radius is $\lambda_1 \le \sqrt{2L - N + 1}$, where equality is reached for the complete graph and the star graph [42]. Since the number of links in the star graph is $L = N - 1$, we obtain $\lambda_1 = \sqrt{N-1}$. For the viral conductance, an expression was derived in [23] by manipulating Eq.(7) as

$$\psi_{K_{1,N-1}} = \frac{\ln N}{2} - \frac{1}{2} + O\left(\frac{1}{\sqrt{N}}\right) \tag{14}$$

which can be written as a function of the spectral radius as

$$\psi_{K_{1,N-1}} = \ln \lambda_1 - \frac{1}{2} + O\left(\frac{1}{\sqrt{\lambda_1^2 - 1}}\right) \tag{15}$$

7. Relationship between robustness metrics in graphs without exact expressions for ψ

There are graph classes that do not have an analytical expression for viral conductance. As such, we compute the Pearson's

[2] https://ams-ix.net/

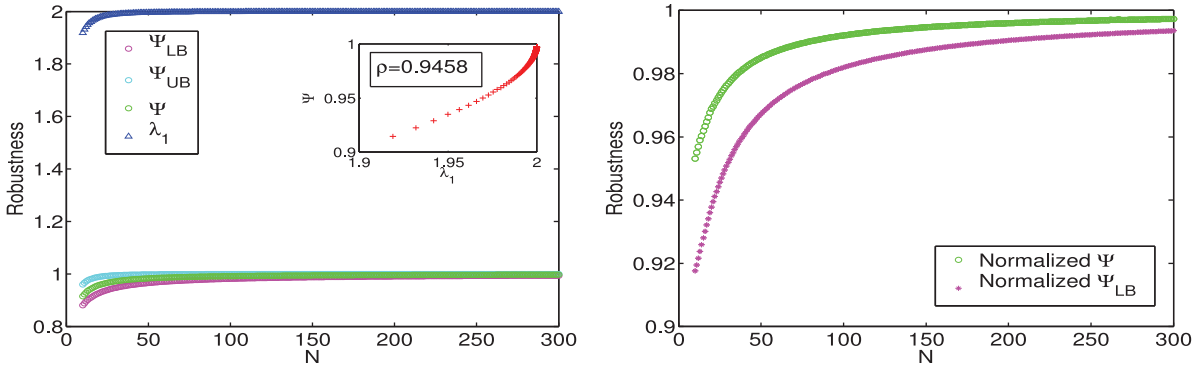

(a) (b)

Fig. 3. (a) Robustness in path graphs. (b) Normalized values of viral conductance ψ and of lower bound ψ_{LB} with respect to upper bound $\psi_{UB} = \lambda_1/2$ value.

correlation coefficient ρ between ψ and λ_1 as $\rho_{\Psi,\lambda_1} = \frac{COV(\Psi,\lambda_1)}{\delta_\Psi \delta_{\lambda_1}}$ where $COV(\Psi, \lambda_1)$ is the covariance between Ψ and λ_1, and δ_Ψ and δ_{λ_1} are the standard deviations. For those graph classes, when computing the steady-state probabilities of being infected for each node, we initialized vector $V(0)$ to all ones, assuming that all nodes are initially infected with probability $v_i(0) = 1$. All the simulations have been performed using MATLAB.

7.1. Path graphs

The path graph is a particularly simple example of a tree graph, where every root node has a branch and only the last root node is not branched at all. As shown in [42], the spectral radius of the path graph is $\lambda_1 = 2\left(1 - \cos\left(\pi \frac{N-1}{N}\right)\right)$. For the viral conductance, we do not have an exact expression, thus we consider a set of graph samples with network size $10 \leq N \leq 300$ and we show the relationship between ψ and λ_1 by plotting ψ (green markers), its lower bound ψ_{LB} (magenta markers) and upper bound ψ_{UB} (cyan markers), and λ_1 (blue markers) versus the number of nodes. Fig. 3(a) shows that the viral conductance of the path graph is very similar to the ring graph where $\psi_{ring} = 1$ for each N. This is expected, because the average fraction of infected nodes in the steady state is about the same in the two graphs. We also verified the validity of lower and upper bounds ψ_{LB} and ψ_{UB}, noticing that for all network sizes ψ is bounded and the difference between ψ and its upper and lower bounds decreases as N increases. The insert in Fig. 3(a) shows that λ_1 and ψ are very strongly correlated for the path graph, having a Pearson's correlation coefficient $\rho = 0.9458$. Fig. 3(b) shows the relationship between ψ and λ_1, as defined in Eq. (10) with respect to the upper and lower bounds, for different network sizes. The viral conductance normalized with respect to the upper bound $\lambda_1/2$ is slightly lower than 1 and the normalized lower bound (which equals $Z + \zeta(1 - Z)$) is close to 1, thus showing that the viral conductance approximately equals half of the spectral radius and confirming the strong relationship between the two robustness metrics.

7.2. Erdős–Rényi random graphs

The Erdős–Rényi random graph $G_p(N)$ can be generated from a set of N nodes by randomly assigning an edge with probability p to each pair of nodes [25]. Besides its analytic tractability, this graph is a reasonably accurate model for peer-to-peer and ad-hoc networks.

A threshold function for the connectivity of the Erdős–Rényi graph is $p_c \approx \ln(N)/N$ for large N. Thus, an Erdős–Rényi graph is almost surely connected if $p > p_c$. In our simulations, we considered a set of graph samples with network size $10 \leq N \leq 200$, we set $p = 2p_c$ and checked each generated Erdős–Rényi graph for connectivity. Fig. 4(a) depicts the viral conductance with its lower and upper bounds, and the spectral radius as a function of the network size N. For each network size N, we generated 10^2 network realizations of Erdős–Rényi random graph. Hence, each point in the plot corresponds to an average value. For large networks, high values of λ_1 cause an epidemic outbreak and very high values of ψ characterize the ease of virus spread within the network. Moreover, ψ_{LB} and ψ_{UB} are accurate. The inserted plot shows a very strong correlation between the two robustness metrics: the resulting Pearson correlation coefficient is $\rho = 0.9978$. We further verified the strong relationship between the viral conductance and the spectral radius by plotting both ψ and its lower bound ψ_{LB} normalized with respect to the upper bound $\lambda_1/2$ as a function of network size. As shown in Fig. 4(b), the normalized viral conductance ranges between 0.8822 and 0.9588 and the normalized lower bound is also high, thus showing that ψ values for this graph type are also near $\lambda_1/2$.

7.3. Watts–Strogatz small-world graphs

The Watts–Strogatz small-world graph [26] can be generated from a ring lattice of N nodes where each node is connected to k nodes, by rewiring each edge with probability p. Within this graph, most of the nodes can be reached within a small number of hops. Moreover, besides the presence of short paths between nodes, a small-world graph also presents a high clustering coefficient feature. The structural properties of Watts–Strogatz small-world graph have been found in several real-world networks, such as mobile contact networks (e.g. Bluetooth, Wi-Fi and Zig-Bee contact networks), neural networks and biological oscillators.

Fig. 5(a) shows the values of ψ_{LB}, ψ_{UB}, ψ and λ_1 for different network sizes in Watts–Strogatz small-world graphs with rewiring probability $p = 0.5$ and $k = 6$. For this set of simulations, we considered again 10^2 realizations for each graph of size N.The viral conductance of this topology shows a behavior similar to the path and the star graph. Here, ψ is almost constant with N, with an average value of 3.06. This means that the number of nodes does not influence the viral conductance of the Watts–Strogatz small world graph with a given rewiring probability. We can further note that the accuracy of upper and lower bounds for the viral conductance is verified and the resulting correlation between ψ and λ_1 is also high ($\rho = 0.9311$). Moreover, Fig. 5(b) shows that the normalized viral conductance ranges between 0.9348 and 0.9777 and the normalized lower bound is also close to 1, thus concluding that the behavior of Watts–Strogatz small-world graphs is similar to path graphs and Erdős–Rényi random graphs, having ψ values very near $\lambda_1/2$.

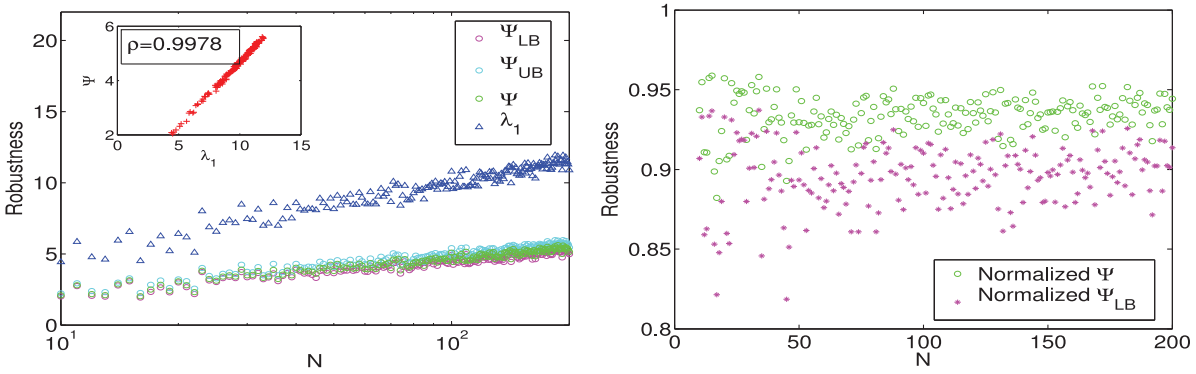

Fig. 4. (a) Robustness in Erdős–Rényi graphs with $p = 2\ln(N)/N$. (b) Normalized values of viral conductance ψ and of lower bound ψ_{LB} with respect to upper bound ψ_{UB}.

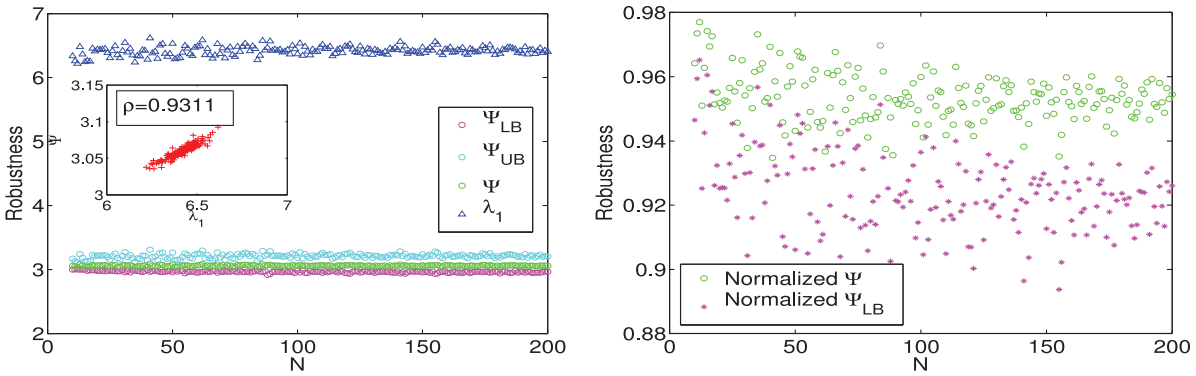

Fig. 5. (a) Robustness in Watts–Strogatz small-world graphs with $p = 0.5$ and $k = 6$. (b) Normalized values of viral conductance ψ and of lower bound ψ_{LB} with respect to upper bound ψ_{UB}.

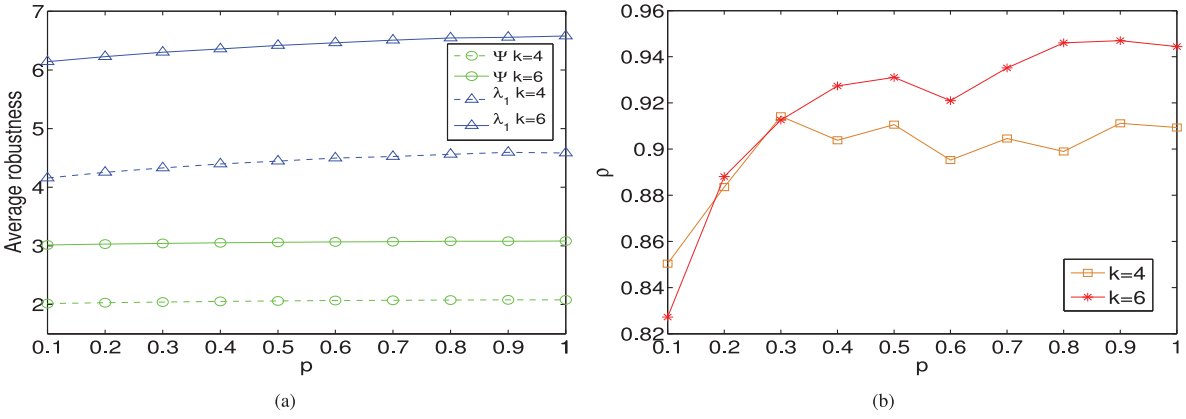

Fig. 6. Watts–Strogatz small-world graphs with $k = 4$ and 6, and rewiring probability $0.1 \le p \le 1$: (a) average robustness and (b) Pearson's correlation coefficient between ψ and τ_c.

The above analysis of the viral conductance versus the spectral radius was also applied to the Watts–Strogatz small-world graphs with other rewiring probabilities and $k = 6$ leading to the same observations as discussed in this subsection. Fig. 6(a) shows the average robustness in Watts–Strogatz small-world graphs with $k = 4$ and 6, and rewiring probability $0.1 \le p \le 1$, while Fig. 6(b) shows the corresponding correlation values. We observe that the values of viral conductance for $k = 6$ are higher than the values with $k = 4$, and also the correlation values for most of the rewiring probabilities are higher for the Watts–Strogatz small-world graphs with $k = 6$.

7.4. Bárabasi–Albert scale-free graphs

The Bárabasi–Albert scale-free graph [27] can be generated starting from m nodes, and at every time step, a new node with m edges is added to m different nodes already present in the graph. The probability that a new node will be connected to an existing node during a certain time step is proportional to the degree of the existing node. This is also referred to as *preferential attachment*. The relevant feature of Bárabasi–Albert scale-free graph is its power-law degree distribution which has been found in many real-world complex networks including the Internet, the World Wide Web, ci-

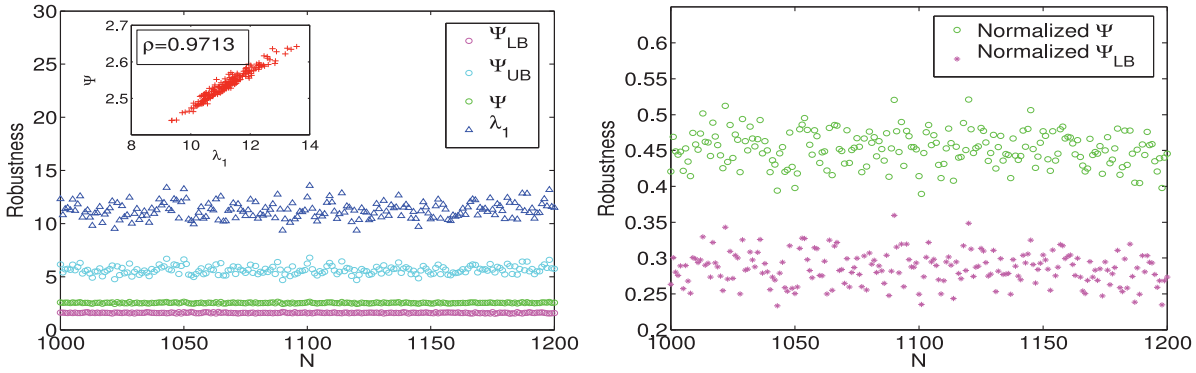

Fig. 7. (a) Robustness in Bárabasi–Albert scale-free graphs with $m = 2$. (b) Normalized values of viral conductance ψ and of lower bound ψ_{LB} with respect to upper bound ψ_{UB} value.

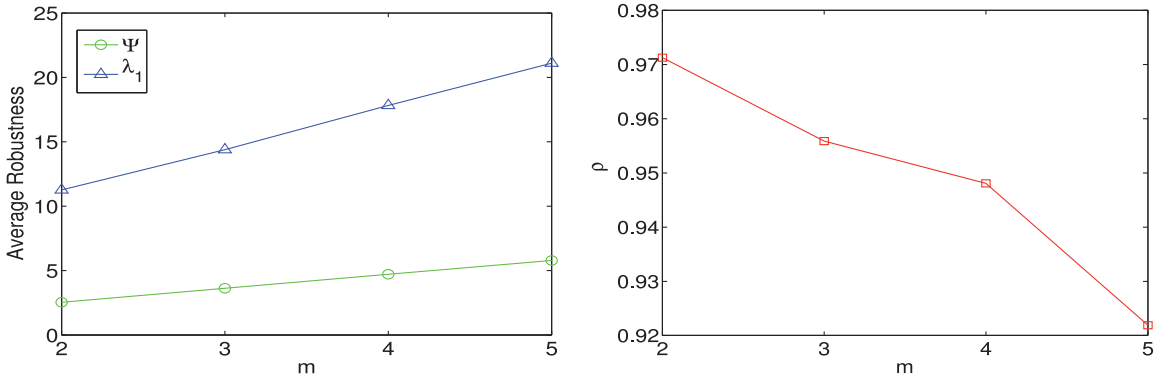

Fig. 8. Bárabasi–Albert scale-free graphs with $m = 2, 3, 4$, and 5: (a) average robustness and (b) Pearson's correlation coefficient between ψ and τ_c.

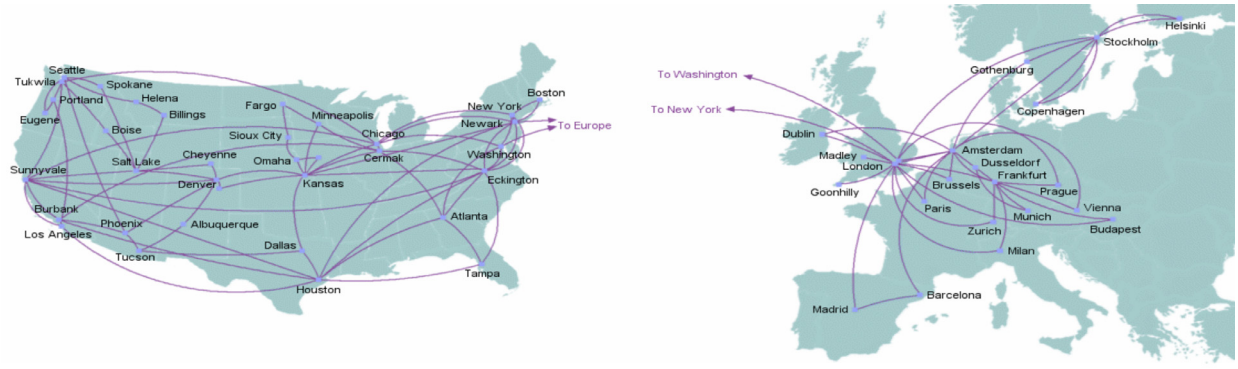

(a) BT North America, 2010 (b) BT Europe, 2010

Fig. 9. BT IP backbone networks within North America and Europe.

tation networks and some social networks. These networks have a high number of nodes (i.e. *hub* nodes) with degree higher than the average degree found in the network.

Fig. 7(a) shows ψ_{LB}, ψ_{UB}, ψ and λ_1 values, and the correlation between ψ and λ_1 for a set of Bárabasi–Albert scale-free graphs with network size $1000 \leq N \leq 1200$ and $m = 2$. For this set of simulations, we generated 10^2 realizations of Bárabasi–Albert scale-free graph for each network size N. We observe that the viral conductance is bounded. However, the lower bound is more accurate than the upper bound. As far as the correlation between the two robustness metrics is concerned, we found again a very strong correlation ($\rho = 0.9713$). Moreover, as shown in Fig. 7(b), the ratio between the viral conductance and the half of spectral radius is significantly lower than the ratio found for the other graph classes analyzed in this work.

To address the differences between ψ and λ_1 for graphs having other m values, we show the average values of ψ and λ_1 for Bárabasi–Albert scale-free graphs having $m = 2, 3, 4$, and 5, which correspond to the average degrees 4, 6, 8 and 10, respectively, in Fig. 8(a). Both the viral conductance and the spectral radius increase as the average graph degree increases. Moreover, the ratio ψ/λ_1 increases with the average degree. Also, we evaluated the

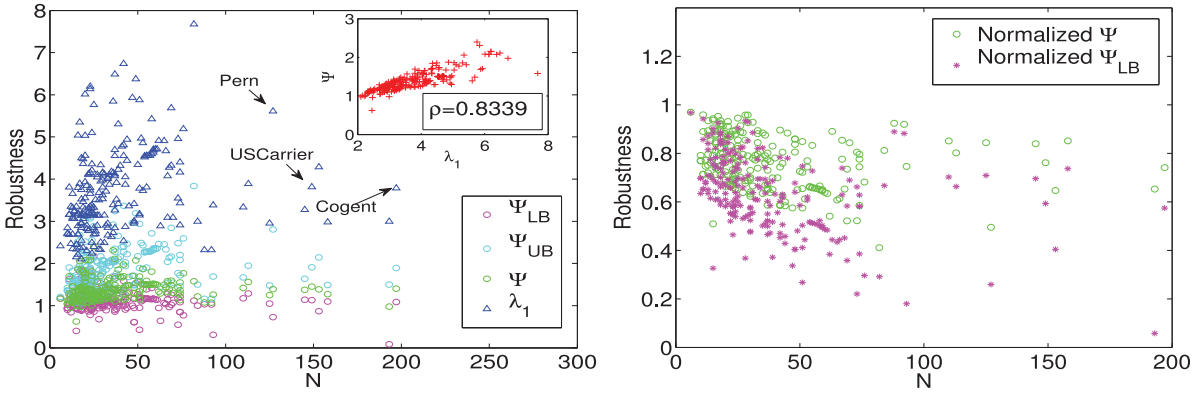

Fig. 10. (a) Robustness in a set of Internet Backbone graphs from the Internet Topology Zoo. (b) Normalized values of viral conductance ψ and of lower bound ψ_{LB} with respect to upper bound ψ_{UB}.

Pearson's correlation coefficient between ψ and λ_1 for different m values. Fig. 8(b) shows a very strong correlation with correlation values decreasing as m increases.

7.5. Real-world graphs: Internet backbones

In this subsection, we consider a set of realistic networks taken from the Internet Topology Zoo[3], a repository containing Internet network topologies coming from all over the world. Most of the network data provided by this website have been created from the information made public by several network operators [44]. As such, it is the most accurate large-scale collection of network topologies currently available. Fig. 9 shows two examples of Internet backbones taken from this repository. Routing attacks on an Internet backbone can affect a large number of hosts, entire networks, or even the global Internet. A compromised BGP router, for example, can modify, drop, or introduce fake BGP updates leading to blackholing, redirection or instability [45].

For this analysis with realistic networks, we considered 236 Internet backbones graphs. The Internet Topology Zoo currently contains more than 250 networks but in our analysis, we did not consider small topologies with less than 7 nodes. Each network topology has been converted from a .gml format to an adjacency matrix in a .mat format using a Python script. In Fig. 10(a), we show ψ_{LB}, ψ_{UB}, ψ and λ_1 values for the set of Internet backbone networks considered. Note that there are networks having the same number of nodes and hence, for a given network size, there can be more robustness values. As can be further observed, most of the networks have a number of nodes ranging from 10 to 75 nodes. We observe again that the lower bound is more accurate than the upper bound. However, differently from the other graphs types, Fig. 10(b) shows that the ratio between the viral conductance and the half of spectral radius is more variable, ranging between 0.4112 and 0.9679. We can further observe that the normalized lower bound for the viral conductance lies around 0.625 on average, with a standard deviation which is higher than in the other graph classes. Here, there are network topologies with normalized Ψ_{LB} close to 0 and with a high normalized Ψ. Looking at Fig. 11, where the Z function and the fundamental weight w_1 are shown, we note that while the w_1 values are medium high for these particular network topologies, thus justifying the high corresponding values of viral conductance, the corresponding Z values are small. Higher values for the fundamental weight, in fact, are representative of network topologies having a high number of infected nodes due to the high cumulative eigenvector centrality measured adding the eigenvector centrality of each node. This lead us to conclude that for these topologies with normalized Ψ_{LB} close to 0, the correction factor K_{min} is needed.

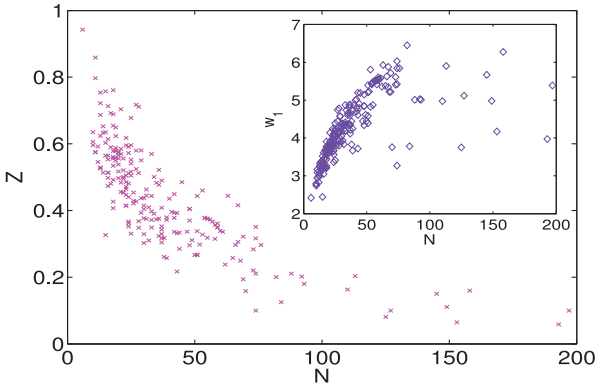

Fig. 11. Z function and the fundamental weight w_1 in the Internet backbone graphs.

Table 1
Spectral radius and viral conductance for some realistic Internet backbone networks.

Network	N	L	E[d]	λ_1	ψ
Pern	127	129	2.0315	5.6133	1.3895
UsCarrier	158	189	2.3924	2.9842	1.2708
Cogent	197	243	0.42	3.7873	1.4036

As far as the correlation between ψ and λ_1 is concerned, we found again a very strong correlation ($\rho = 0.8339$). However, the correlation value found is the lowest compared to the other graph classes. This means that there may be some cases (with low probability to occur considering that the correlation is very strong) in which epidemic threshold may fail to assess network robustness. In Fig. 10(a), we also highlighted some networks that are interesting to analyze. In Table 1, we summarize their characteristics in terms of network size, number of links, average degree and robustness values. Comparing Cogent and UsCarrier, for example, both ψ and λ_1 consider UsCarrier as the most robust backbone. On the contrary, comparing Cogent and Pern, the viral conductance considers Cogent as the most robust, while the spectral radius considers Pern as the most robust.

[3] http://www.topology-zoo.org/

8. Conclusions

This paper has studied the relationship between the viral conductance Ψ and the spectral radius λ_1 which is the inverse of the NIMFA epidemic threshold $\tau_c^{(1)}$ in networks. Through examples, we have described how the two metrics quantify network robustness with respect to the spread of SIS epidemics and showed cases in which the viral conductance better assesses network robustness. However, even if the viral conductance provides more information about network's behavior with respect to the spread of a virus, we have shown that this more complete information is not always necessary.

For conducting our analysis, we have chosen as target network graphs those modeling the most widely diffused telecommunication networks (e.g. complete bipartite graphs for core telecommunication networks, Erdős–Rényi random graphs for peer-to-peer and ad hoc networks, Watts–Strogatz small-world graphs for mobile contact networks, Bárabasi–Albert scale-free graphs for social networks, etc.) and a set of real-world Internet backbones. Our correlation analysis, while limited to a set of topologies, revealed that in regular graphs, complete bipartite graphs, path graphs, Erdős–Rényi random graphs, Watts–Strogatz small-world graphs, Bárabasi–Albert scale-free graphs and Internet backbone graphs the viral conductance and the spectral radius are highly correlated thus concluding that Ψ is generally close to $\alpha\lambda_1/2$ with α close to 1 but smaller. Hence, when comparing networks of the same class, the spectral radius is adequate for comparing network robustness. The extension of this result proving the high correlation between the two robustness metrics to other network classes remains an open question. For future work, we will explicitly focus on this research direction.

Acknowledgment

This work has been partially supported by the European Commission, European Social Fund 2007/2013 and Calabria Region-ARUE grant. The authors would like to thank Faryad Darabi Sahneh for the insightful suggestions.

References

[1] R.M. Anderson, R.M. May, Infectious Diseases of Humans, vol. 1, Oxford University Press, Oxford, 1991.
[2] J.O. Kephart, S.R. White, Directed-graph epidemiological models of computer viruses, in: IEEE Computer Society Symposium on Research in Security and Privacy, IEEE, 1991, pp. 343–359.
[3] Z. Chen, C. Ji, Spatial-temporal modeling of malware propagation in networks, Neural Netw. IEEE Trans. 16 (5) (2005) 1291–1303.
[4] A.L. Lloyd, R.M. May, How viruses spread among computers and people, Science 292 (5520) (2001) 1316–1317.
[5] E. Yoneki, P. Hui, J. Crowcroft, Wireless epidemic spread in dynamic human networks, in: Bio-Inspired Computing and Communication, Springer, Berlin, Heidelberg, 2008, pp. 116–132.
[6] D. Chakrabarti, J. Leskovec, C. Faloutsos, S. Madden, C. Guestrin, M. Faloutsos, Information survival threshold in sensor and P2P networks, in: INFOCOM 2007. 26th IEEE International Conference on Computer Communications., IEEE, 2007, pp. 1316–1324.
[7] E.G. Coffman Jr, Z. Ge, V. Misra, D. Towsley, Network resilience: exploring cascading failures within BGP, in: Proc. 40th Annual Allerton Conference on Communications, Computing and Control, 2002.
[8] Y. Koç, M. Warnier, P. Van Mieghem, R.E. Kooij, F.M.T. Brazier, A topological investigation of phase transitions of cascading failures in power grids, Physica A Stat. Mech. Appl. 415 (2014) 273–284.
[9] S. Peng, S. Yu, A. Yang, Smartphone malware and its propagation modeling: A survey, Commun. Surv. Tut. IEEE 16 (2) (2014) 925–941.
[10] P. De, Y. Liu, S.K. Das, An epidemic theoretic framework for vulnerability analysis of broadcast protocols in wireless sensor networks, Mobile Comput. IEEE Trans. 8 (3) (2009) 413–425.
[11] P. Van Mieghem, J. Omic, R.E. Kooij, Virus spread in networks, IEEE/ACM Trans. Netw. 17 (1) (2009) 1–14.
[12] A. Ganesh, L. Massoulié, D. Towsley, The effect of network topology on the spread of epidemics, in: INFOCOM 2005. 24th Annual Joint Conference of the IEEE Computer and Communications Societies. Proceedings IEEE, vol. 2, IEEE, 2005, pp. 1455–1466.
[13] Y. Wang, D. Chakrabarti, C. Wang, C. Faloutsos, Epidemic spreading in real networks: an eigenvalue viewpoint, in: 22nd International Symposium on Reliable Distributed Systems, IEEE, 2003, pp. 25–34.
[14] D. Chakrabarti, Y. Wang, C. Wang, J. Leskovec, C. Faloutsos, Epidemic thresholds in real networks, ACM Trans. Inf. Syst. Security (TISSEC) 10 (4) (2008) 1–26.
[15] C. Li, R. van de Bovenkamp, P. Van Mieghem, Susceptible-infected-susceptible model: a comparison of n-intertwined and heterogeneous mean-field approximations, Phys. Rev. E 86 (2) (2012) 026116.
[16] R. Pastor-Satorras, C. Castellano, P. Van Mieghem, A. Vespignani, Epidemic processes in complex networks, Rev. Modern phys. 87 (3) (2015) 925.
[17] N.T. Bailey, et al., The Mathematical Theory of Infectious Diseases and its Applications, Charles Griffin & Company Ltd, 5a Crendon Street, High Wycombe, Bucks HP13 6LE., High Wycombe, 1975.
[18] D.J. Daley, J. Gani, J.M. Gani, Epidemic modelling: an introduction, vol. 15, Cambridge University Press, Cambridge, 2001.
[19] V.M. Eguiluz, K. Klemm, Epidemic threshold in structured scale-free networks, Phys. Rev. Lett. 89 (10) (2002) 108701.
[20] A. Jamakovic, R.E. Kooij, P. Van Mieghem, E.R. van Dam, Robustness of networks against viruses: the role of the spectral radius, in: Symposium on Communications and Vehicular Technology, IEEE, 2006, pp. 35–38.
[21] R.E. Kooij, P. Schumm, C. Scoglio, M. Youssef, A new metric for robustness with respect to virus spread, in: NETWORKING 2009, Springer, Berlin, Heidelberg, 2009, pp. 562–572.
[22] M. Youssef, R.E. Kooij, C. Scoglio, Viral conductance: Quantifying the robustness of networks with respect to spread of epidemics, J. Comput. Sci. 2 (3) (2011) 286–298.
[23] P. Van Mieghem, The viral conductance of a network, Comput. Commun. 35 (12) (2012) 1494–1506.
[24] M. Draief, A. Ganesh, L. Massoulié, Thresholds for virus spread on networks, in: Proceedings of the 1st international conference on Performance evaluation methodolgies and tools, ACM, 2006, p. 51.
[25] P. Erdos, A. Rényi, On the evolution of random graphs, Publ. Math. Inst. Hung. Acad. Sci 5 (1960) 17–61.
[26] D.J. Watts, S.H. Strogatz, Collective dynamics of small-world networks, Nature 393 (6684) (1998) 440–442.
[27] A. Barabási, R. Albert, Emergence of scaling in random networks, Science 286 (5439) (1999) 509–512.
[28] M.J. Keeling, K.T. Eames, Networks and epidemic models, J. R. Soc. Interface 2 (4) (2005) 295–307.
[29] O. Diekmann, J.A.P. Heesterbeek, Mathematical epidemiology of infectious diseases, vol. 146, Wiley, Chichester, 2000.
[30] V.M. Preciado, M. Zargham, C. Enyioha, A. Jadbabaie, G. Pappas, Optimal vaccine allocation to control epidemic outbreaks in arbitrary networks, in: Decision and Control (CDC), 2013 IEEE 52nd Annual Conference on, IEEE, 2013, pp. 7486–7491.
[31] S. Bonaccorsi, S. Ottaviano, F. De Pellegrini, A. Socievole, P. Van Mieghem, Epidemic outbreaks in two-scale community networks, Physical Review E 90 (1) (2014) 012810.
[32] S. Bonaccorsi, S. Ottaviano, D. Mugnolo, F.D. Pellegrini, Epidemic outbreaks in networks with equitable or almost-equitable partitions, SIAM Journal on Applied Mathematics 75 (6) (2015) 2421–2443.
[33] Y. Hayel, Q. Zhu, Resilient and secure network design for cyber attack-induced cascading link failures in critical infrastructures, in: Information Sciences and Systems (CISS), 2015 49th Annual Conference on, IEEE, 2015, pp. 1–3.
[34] M. Manzano, E. Calle, J. Ripoll, A.M. Fagertun, V. Torres-Padrosa, Epidemic survivability: characterizing networks under epidemic-like failure propagation scenarios, in: Design of Reliable Communication Networks (DRCN), 2013 9th International Conference on the, IEEE, 2013, pp. 95–102.
[35] S. Trajanovski, S. Scellato, I. Leontiadis, Error and attack vulnerability of temporal networks, Phys. Rev. E 85 (6) (2012) 066105.
[36] S. Trajanovski, F. Kuipers, A. Ilic, J. Crowcroft, P. Van Mieghem, et al., Finding critical regions and region-disjoint paths in a network, IEEE/ACM Trans. Netw. 23 (3) (2015) 908–921.
[37] P. Van Mieghem, C. Doerr, H. Wang, J. Martín Hernández, D. Hutchison, M. Karaliopoulos, R.E. Kooij, A Framework for Computing Topological Network Robustness, Report 20101218, Delft University of Technology, 2010.
[38] M. Manzano, F. Sahneh, C. Scoglio, E. Calle, J.L. Marzo, Robustness surfaces of complex networks, Nature Sci. Rep. 4 (2014).
[39] S. Trajanovski, J. Martín Hernández, W. Winterbach, P. Van Mieghem, Robustness envelopes of networks, J. Complex Netw. 1 (1) (2013) 44–62.
[40] E. Cator, P. Van Mieghem, Second-order mean-field susceptible-infected-susceptible epidemic threshold, Phys. Rev. E 85 (5) (2012) 056111.
[41] P. Van Mieghem, R. Van de Bovenkamp, Accuracy criterion for the mean–field approximation in susceptible-infected-susceptible epidemics on networks, Phys. Rev. E 91 (3) (2015) 032812.
[42] P. Van Mieghem, Graph Spectra for Complex Networks, Cambridge University Press, Cambridge, 2011.
[43] C. Li, H. Wang, P. Van Mieghem, New lower bounds for the fundamental weight of the principal eigenvector in complex networks, Third International IEEE Workshop on Complex Networks and their Applications, November 23-27, Marrakesh, Morocco, 2014.
[44] S. Knight, H.X. Nguyen, N. Falkner, R. Bowden, M. Roughan, The Internet topology zoo, IEEE J. Sel. Areas Commun. 29 (9) (2011) 1765–1775.
[45] O. Nordström, C. Dovrolis, Beware of BGP attacks, ACM SIGCOMM Comput. Commun. Rev. 34 (2) (2004) 1–8.

Annalisa Socievole is a Research Fellow in the DIMES department at University of Calabria, Italy. She received a PhD in Systems and Computer Science Engineering in February 2013 and a master's degree in Telecommunications Engineering in July 2009, both from University of Calabria. From October 2011 to April 2012 she has been a visiting PhD student in the Systems Research Group of Cambridge Computer Laboratory (UK). From November 2013 to June 2014 she spent a Post-doc period in NAS Group at TU Delft (NL) to carry out the research project CONTACTO. Her research interests include Opportunistic Networks and Complex Networks.

Floriano De Rango is an Assistant Professor in the DIMES department at University of Calabria, Italy. He received a degree in Computer Science Engineering in October 2000, and a PhD in Electronics and Communications Engineering in January 2005, both at University of Calabria. From March to November 2004 he was visiting researcher at the University of California, Los Angeles (UCLA). From November 2004 until September 2007 he was a Research Fellow in the DEIS Department at University of Calabria. His interests include Satellite networks, IP QoS architectures, Adaptive Wireless Networks, Ad Hoc Networks and Pervasive Computing.

Caterina M. Scoglio is a Professor of Electrical and Computer Engineering at Kansas State University. Her main research interests are in the field of network science and engineering. She received the Dr. Eng. degree from the "Sapienza" Rome University, Italy, in 1987. Before joining Kansas State University, she worked at the Fondazione Ugo Bordoni from 1987 to 2000, and at the Georgia Institute of Technology from 2000 to 2005. Caterina is also core faculty at the Institute of Computational Comparative Medicine (ICCM).

Piet Van Mieghem received the Masters (magna cum laude, 1987) and PhD (summa cum laude, 1991) degrees in electrical engineering from the K.U. Leuven, Belgium. He is a Professor at the Delft University of Technology and Chairman of the section Network Architectures and Services (NAS) since 1998. His research interests include modeling and analysis of complex networks and new Internet-like architectures and algorithms for future communications networks. Before joining Delft, he worked at the Interuniversity Micro Electronic Center (IMEC) from 1987 to 1991. During 1993 to 1998, he was a member of the Alcatel Corporate Research Center in Antwerp, Belgium.